Astron. Astrophys. 247, 565–575 (1991)

ASTRONOMY
AND
ASTROPHYSICS

The orbits of Triton and Nereid from spacecraft and Earthbased observations

R.A. Jacobson[1], **J.E. Riedel**[1], **and A.H. Taylor**[1]

301-150 Jet Propulsion Laboratory, California Institute of Technology, 4800 Oak Grove Drive, Pasadena, CA 91109, USA

Received November 27, accepted December 14, 1990

Abstract. In this paper we discuss the determination of improved orbits for the Neptunian satellites Triton and Nereid. Our primary results are the final set of model parameters which generate orbits that best fit both the Earthbased satellite observations and data acquired by the Voyager spacecraft during the Neptune encounter. We assess the accuracy of the improved orbits and compare them with the orbits generated prior to the encounter. We also provide mean elements as a geometrical representation for the orbits.

Key words: astrometry – celestial mechanics – Nereid; satellites of Neptune – Triton

1. Introduction

On August 25, 1989 the Voyager 2 spacecraft completed its tour of the outer planets with a passage through the Neptunian system. The spacecraft performed numerous scientific observations of the planet and its satellites. Key contributors to the high quality of those observations were the accurate navigation of the spacecraft and the precise pointing of the science instruments. Both the navigation and the pointing depended upon knowledge of the positions of the Neptunian satellites.

In earlier papers, Jacobson (1987, Paper I; 1990, Paper II), discussed the determination of the orbits of Triton and Nereid prior to the Voyager encounter. Those orbits were predicted to be in error by as much as 1100 km for Triton and 200,000 km for Nereid. The error was due to the limited accuracy of the observations used in the orbit determination and the poorly known physical constants (e.g. Neptune and Triton GM's, Neptune J_2) used in the orbital motion model. The orbits of Paper II were the basis for the initial operational satellite ephemerides adopted by the Voyager Project. Because of the size of their error, however, the ephemerides could not be used to support the encounter. Consequently, the orbits had to be improved during the approach to Neptune and revised ephemerides had to be generated. The Voyager navigation data, which was highly accurate and also sensitive to the satellite positions as well as the unknown constants, provided the information for the orbital improvement.

Send offprint requests to: R.A. Jacobson

Beginning with the Observatory Phase of the mission (81 days before Neptune closest approach) periodic updates of the orbits became part of the real time navigation process. In effect, the spacecraft and satellites were navigated together. Each time a revised estimate of the spacecraft trajectory was delivered to the Voyager project, it was accompanied by revised ephemerides for the satellites. The procedure was essentially identical to the one used during the Voyager Uranus encounter (Jacobson 1986; Taylor 1986; Synnott 1986).

In this paper we focus on the post-encounter determination of the Triton and Nereid orbits. The results include the set of state vectors and dynamical constants which generate the orbits that best fit the combined set of Voyager data and Earthbased data. The postfit residuals for all of the data are graphically displayed and their statistics tabulated to show the quality of the fit. A comparison of the post-encounter orbits with those from Paper II is also presented and the accuracy of the post-encounter orbits is assessed. Finally we give a set of mean elements to aid in the geometric interpretation of the orbits and in comparisons with orbits obtained by other investigators.

2. Satellite orbit model

The model for the satellite orbits is numerical integration of their equations of motion. Those equations include the gravitational effects of the oblate primary, the mutual perturbations of the satellites, and a perturbation due to a body which approximates the perturbations of the solar system bodies external to the Neptunian system. The external body is a fictitious body located at the solar system barycenter and having a GM equal to the sum of the GM's of the bodies interior to Neptune. In the description of the oblateness force, the pole of Neptune is represented by a unit vector precessing at a constant rate about an axis aligned with the Neptunian system angular momentum vector. The dynamical model is identical to that used for the pre-encounter orbits and is discussed in detail in Papers I, II, and Peters (1981). Appendix A gives the expression for the system angular momentum.

3. Satellite orbit determination

We determined the satellite orbits by performing a least squares fit to observations subject to a linear equality constraint. The

latter enforced the alignment of the Neptune pole precession axis and the system angular momentum vector. Estimated parameters included the satellite epoch states, planetary system GM, Triton GM, Neptune J_2, Neptune J_4, Neptune pole, the pole precession axis, the pole precession rate, the magnitude of the Neptunian system angular momentum, and the Voyager spacecraft state.

Papers I and II give two different formulations for the angular momentum constraint. The current fit, however, used neither but instead simply required that, in a least squares sense, the angular momentum vector be constant in magnitude and be aligned with the precession axis over the time spanned by the observations. The direct elimination technique described by Lawson & Hanson (1974) introduced the constraint into the data fit. In that technique a subset of the estimated parameters is found directly from the constraint. For the current fit the subset contained the angular momentum magnitude, the precession axis orientation angles, and the precession rate.

The observations in the fit were Earthbased astrometric observations, optical observations made by the Voyager spacecraft, the Triton occultation of the spacecraft observed by the Voyager Radio Science Team (RSS), the Triton occultation of the star β Canis Majoris observed by the Voyager Ultraviolet Spectrometer (UVS), and all of the Voyager radiometric tracking data used in the post-encounter spacecraft trajectory reconstruction (see Lewis 1990 for a discussion of that reconstruction). The 1988 Voyager observations used in the pre-encounter orbit determination were not fit.

The astrometric observations of Triton included all of the available observations, both visual and photographic, in the 141 years from 1847 to 1988. The astrometric observations of Nereid, all photographic, covered the 39 year period from 1949 to 1988. The source of the astrometric observations was the open literature and private communications with observers at the U.S. Naval Observatory and the Royal Greenwich Observatory. Paper II discusses in more detail the observations and problems associated with their processing. The current analysis uses all of the observations used in the analysis in Paper II plus two additional Nereid observations provided by D. Pascu of the U.S. Naval Observatory (private communication 1989).

The occultation observations, provided by the respective Voyager RSS and UVS science teams (Marouf 1990; Holberg 1990), were the times of occultation ingress and egress. These observations have the potential to fix Triton's position very accurately. However, they are limited by knowledge of Triton's radius which, from Voyager imaging data, is presumed known only to the 7 km level (Riedel 1990).

The radiometric tracking data are a source of information on a number of key Neptunian system dynamical parameters. Among them are the system and Triton GM's, Neptune zonal harmonics, and Neptune pole orientation angles. These parameters were all poorly known pre-encounter, and determination of their values was crucial to improvement of the satellite orbits.

We set the weights of the astrometric observations separately for each observer at each opposition according to the RMS of the residuals. For most of the Triton and Nereid optical observations from Voyager the weights were 0.5 pixel. However, the weights for the early Nereid observations were 2.0 pixels because those observations were made with long exposures causing the observed images to smear, and the weights of the late Triton observations gradually increased (from 0.5 to 2.0 pixel) as the size of the Triton image increased making centerfinding difficult. The weights on the RSS Triton occultation were 0.02 s, on the UVS occultation ingress was 3.0 s, and on the UVS occultation egress was 0.32 s. The weights on the Voyager radiometric data were the same as those used in the spacecraft trajectory reconstruction.

The Nereid astrometric observations contain systematic errors. To reduce the effect of those errors, we included as estimated parameters observation biases for each observer. The data fitting process treated the biases as batch sequential white noise parameters where a batch contained all the observations at a particular opposition. This estimation technique is analogous to using distinct biases for each batch (Bierman 1978). The Triton Earthbased observations are also corrupted by systematic errors. However, as shown in Paper II, they have a negligible effect on the determination of the orbit and may be safely ignored.

Tables 1 and 2 give the RMS of the post-fit observation residuals, grouped by observer and opposition, for the respective satellites. The entries in each table provide a concise summary of the number and type observations and their accuracy. Position angle and separation distance observations are denoted by p and s; relative right ascension and declination observations are denoted by $\Delta\alpha$ and $\Delta\delta$. For consistency with the other observations, the RMS of the Voyager optical observations is given in seconds of arc rather than lines and pixels. The statistics of the residuals for the Voyager radiometric data, not included in the tables, are unchanged from those found by Lewis (1990) during the spacecraft trajectory reconstruction. The Triton residuals are slightly larger than those quoted in Paper II because of the absence of observer biases in the current fit.

Figures 1–4 are time histories of the Earthbased observation residuals with the position angle and separation distance residuals converted into equivalent differential right ascension and declination residuals for display. Figures 5–8 are the optical residual time histories. These figures give an indication of the variation in quality and the overall time distribution of the observations.

4. Epoch state vectors and dynamical parameters

Tables 3 and 4 contain the values of the satellite epoch state vectors and the system dynamical constants. We specify the vector components and parameters to eighteen digits to enable their use in future orbit integrations. Note that the epoch of the state vectors is 3 June 1989 whereas the epoch of the states in Paper II was 1 November 1987. Values of the dynamical constants required in the integration but not determined in the fit also appear in Table 4; all except the external perturbing body GM are those officially adopted by the Voyager Project (Gerschultz 1989). The external body GM is equal to the sum of the GM's of the bodies interior to Neptune with the GM's of those bodies taken from JPL planetary ephemeris DE130.

In Table 4 the uncertainties for the system GM, the Triton GM, the Neptune zonal harmonics, the Neptune pole parameters, and the precession axis parameters are our estimate of the actual $1-\sigma$ statistics. They were determined from an examination of the formal statistics and from an evaluation of the changes in the parameter values for differing data sets, data weights, and estimated parameter sets. Note that the precession axis orientation is slightly more uncertain than the Neptune pole orientation. The precession axis orientation is determined from the precession of Triton's orbit and is related to the Neptune pole orientation

Table 1. Triton observation residual statistics

Opp.	Observer	No.	Type	RMS	No.	Type	RMS
1847	Bond	7	p	2″.73	7	s	0″.979
	Lassel	9	p	2″.23	7	s	0″.442
1848	Bond	10	p	4″.07	10	s	0″.551
	Lassell	3	p	1″.56	1	s	1″.05
1849	Lassell	5	p	1″.34	4	s	1″.07
1850	Lassell	11	p	2″.32	5	s	0″.734
1851	Lassell	6	p	1″.80	3	s	0″.625
1852	Lassell	23	p	2″.45	22	s	0″.744
1863	Lassell/Marth	14	p	1″.33	5	s	0″.544
1864	Lassell/Marth	41	p	1″.72	18	s	0″.695
1873	Newcomb	24	p	1″.59	43	s	0″.253
1874	Newcomb	26	p	0″.775	48	s	0″.539
1875	Hall	21	p	1″.51	20	s	0″.299
	Holden	23	p	1″.72	20	s	0″.469
1876	Hall	6	p	0″.917	6	s	0″.270
	Holden	15	p	1″.27	8	s	0″.346
1877	Holden	8	p	1″.03	9	s	0″.392
1878	Holden	2	p	2″.04	2	s	0″.535
1881	Hall	31	p	0″.877	29	s	0″.177
1882	Hall	11	p	0″.844	13	s	0″.143
1883	Hall	23	p	1″.49	20	s	0″.133
	Henry	8	p	1″.85	12	s	0″.731
1885	Struve, H.	6	p	0″.906	5	s	0″.430
1886	Perrotin	13	p	0″.774	13	s	0″.299
	Struve, H.	15	p	1″.06	15	s	0″.228
1887	Struve, H.	25	p	0″.968	22	s	0″.221
1888	Struve, H.	64	p	0″.861	51	s	0″.235
1889	Parrish	7	p	1″.79	5	s	0″.399
	Struve, H.	20	p	0″.899	20	s	0″.148
1890	Struve, H.	30	p	0″.567	23	s	0″.248
1891	Hall	27	p	1″.50	25	s	0″.460
	Struve, H.	19	p	0″.733	16	s	0″.361
1892	Barnard	8	p	0″.516	9	s	0″.262
	Struve, H.	17	p	0″.575	15	s	0″.211
1893	Barnard	9	p	0″.509	10	s	0″.190
1894	Barnard	14	p	0″.932	14	s	0″.136
	Brown	13	p	0″.572	13	s	0″.226
	Schaeberle	10	p	0″.509	10	s	0″.180
1895	Schaeberle	15	p	0″.595	12	s	0″.100
1896	Brown	1	p	1″.05	1	s	0″.056
	Drew	45	p	1″.65	40	s	0″.366
	Schaeberle	7	p	0″.387	7	s	0″.160
1897	Barnard	53	p	0″.984	53	s	0″.230
	Brown	39	p	0″.647	40	s	0″.248
	Schaeberle	16	p	0″.500	16	s	0″.170
1898	Aitken	13	p	1″.04	13	s	0″.289
	Barnard	54	p	0″.743	54	s	0″.209
	Drew	12	p	0″.952	12	s	0″.308
	Hussey	12	p	0″.747	12	s	0″.289
	Kostinsky	7	p	0″.604	7	s	0″.310
1899	Barnard	72	p	0″.767	71	s	0″.182
	Greenwich	2	p	0″.746	2	s	0″.464
	Hussey	8	p	0″.653	8	s	0″.423
	Kostinsky	7	p	0″.975	7	s	0″.253
	See	62	p	1″.19	64	s	0″.360
1900	Barnard	48	p	0″.883	47	s	0″.231
	Kostinsky	5	p	1″.47	5	s	0″.578

Table 1 (continued)

Opp.	Observer	No.	Type	RMS	No.	Type	RMS
1901	Aitken	9	p	0°.480	13	s	0″.187
	Barnard	47	p	0°.813	47	s	0″.238
	Greenwich	51	p	0°.909	51	s	0″.208
	Perrine	51	p	1°.36	51	s	0″.211
1902	Barnard	27	p	0°.686	27	s	0″.240
	Dinwiddie	22	p	1°.35	22	s	0″.332
	Greenwich	69	p	1°.13	69	s	0″.259
	Wirtz	10	p	2°.82	10	s	0″.475
1903	Barnard	22	p	1°.01	22	s	0″.274
	Dinwiddie	7	p	1°.05	8	s	0″.279
	Greenwich	54	p	0°.670	54	s	0″.217
	Wirtz	2	p	4°.25	2	s	1″.02
1904	Barnard	15	p	0°.707	15	s	0″.282
	Greenwich	57	p	0°.918	57	s	0″.250
	Hammond	11	p	0°.802	10	s	0″.258
	Rice	6	p	0°.830	6	s	0″.318
	Wirtz	1	p	1°.06	1	s	0″.078
1905	Barnard	11	p	0°.993	10	s	0″.360
	Greenwich	63	p	1°.06	63	s	0″.239
	Hammond	29	p	0°.669	30	s	0″.226
	Wirtz	19	p	3°.34	19	s	0″.631
1906	Barnard	17	p	0°.492	16	s	0″.145
	Greenwich	31	p	0°.815	31	s	0″.208
1907	Barnard	24	p	0°.747	25	s	0″.202
	Hammond	13	p	0°.648	13	s	0″.228
	Greenwich	26	p	1°.24	26	s	0″.294
1908	Barnard	26	p	0°.795	25	s	0″.215
	Hall, Jr.	27	p	0°.875	23	s	0″.425
1909	Barnard	25	p	0°.984	25	s	0″.315
	Greenwich	58	p	0°.702	59	s	0″.178
	Hall, Jr.	32	p	0°.900	32	s	0″.302
	Wirtz	1	p	0°.307	1	s	0″.078
1910	Barnard	25	p	1°.02	23	s	0″.271
	Burton	19	p	0°.943	19	s	0″.232
	Hall, Jr.	19	p	0°.781	16	s	0″.221
1911	Barnard	18	p	0°.845	18	s	0″.215
	Burton	44	p	0°.593	44	s	0″.182
1912	Barnard	31	p	0°.810	31	s	0″.275
	Burton	29	p	0°.676	29	s	0″.186
	Hall, Jr.	19	p	1°.00	19	s	0″.283
1913	Barnard	17	p	1°.15	17	s	0″.260
1914	Barnard	5	p	1°.29	5	s	0″.219
1915	Barnard	27	p	0°.840	25	s	0″.237
1916	Barnard	35	p	0°.810	35	s	0″.265
1917	Barnard	21	p	1°.12	22	s	0″.246
1918	Barnard	22	p	0°.833	23	s	0″.227
	Hall, Jr.	25	p	1°.22	25	s	0″.315
1919	Barnard	20	p	1°.00	20	s	0″.189
	Hall, Jr.	18	p	0°.853	18	s	0″.340
1920	Barnard	27	p	1°.18	27	s	0″.208
	Hall, Jr.	22	p	0°.933	23	s	0″.395
1921	Barnard	27	p	0°.936	25	s	0″.254
	Burton	3	p	0°.891	3	s	0″.129
	Hall, Jr.	3	p	0°.762	3	s	0″.504
1922	Hall, Jr.	12	p	1°.05	12	s	0″.319
1924	Hall, Jr.	11	p	1°.06	9	s	0″.355
1925	Hall, Jr.	4	p	0°.613	5	s	0″.376

Table 1 (continued)

Opp.	Observer	No.	Type	RMS	No.	Type	RMS
1927	Burton	9	p	0°.300	9	s	0″.207
	Hall, Jr.	4	p	0°.697	5	s	0″.311
	Crawford	11	p	0°.954	11	s	0″.245
1928	Burton	11	p	0°.991	11	s	0″.234
	Hall, Jr.	3	p	1°.13	3	s	0″.590
1931	Burton	28	p	0°.644	28	s	0″.194
1932	Bower	12	p	0°.637	12	s	0″.151
1936	Burton	16	p	0°.387	16	s	0″.150
	Lyons	20	p	0°.761	21	s	0″.317
1939	Alden	30	p	0°.365	30	s	0″.076
1940	Alden	21	p	0°.300	21	s	0″.101
1941	Burton	2	p	0°.397	2	s	0″.261
	Lyons	23	p	0°.882	24	s	0″.288
	Raynsford	7	p	2°.10	7	s	0″.637
1942	Alden	22	p	0°.334	22	s	0″.099
	Burton	21	p	0°.852	21	s	0″.144
1943	Burton	9	p	0°.467	9	s	0″.128
	USNO unknown	13	p	0°.668	13	s	0″.182
1947	Lyons	6	p	0°.849	6	s	0″.582
1975	Walker	18	$\Delta\alpha \cos\delta$	0″.053	18	$\Delta\delta$	0″.099
1977	Walker	10	$\Delta\alpha \cos\delta$	0″.081	10	$\Delta\delta$	0″.060
1979	Harrington	20	$\Delta\alpha \cos\delta$	0″.029	20	$\Delta\delta$	0″.040
1980	Harrington	16	$\Delta\alpha \cos\delta$	0″.022	16	$\Delta\delta$	0″.016
1981	Harrington	32	$\Delta\alpha \cos\delta$	0″.027	32	$\Delta\delta$	0″.095
1982	Harrington	27	$\Delta\alpha \cos\delta$	0″.029	27	$\Delta\delta$	0″.027
1983	Harrington	17	$\Delta\alpha \cos\delta$	0″.019	17	$\Delta\delta$	0″.022
1984	Harrington	4	$\Delta\alpha \cos\delta$	0″.017	4	$\Delta\delta$	0″.011
1985	Harrington	28	$\Delta\alpha \cos\delta$	0″.023	28	$\Delta\delta$	0″.022
1986	Harrington	24	$\Delta\alpha \cos\delta$	0″.016	24	$\Delta\delta$	0″.029
1987	Landgraf	5	$\Delta\alpha \cos\delta$	0″.497	5	$\Delta\delta$	0″.650
	Walker	28	$\Delta\alpha \cos\delta$	0″.024	28	$\Delta\delta$	0″.037
1988	Walker	14	$\Delta\alpha \cos\delta$	0″.015	14	$\Delta\delta$	0″.040
	Taylor	7	$\Delta\alpha$	0″.047	7	$\Delta\delta$	0″.065
	Williams	6	p	0°.183	6	s	0″.077
1989	VGR Optical	359	pixel	0″.280	359	line	0″.219
	VGR RSS Occ	1	time	0ˢ.000	1	time	0ˢ.001
	VGR star Occ	1	time	0ˢ.940	1	time	0ˢ.070

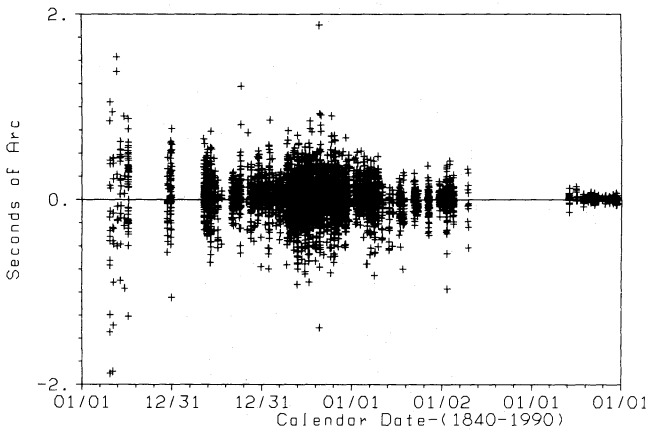

Fig. 1. Triton relative right ascension residuals

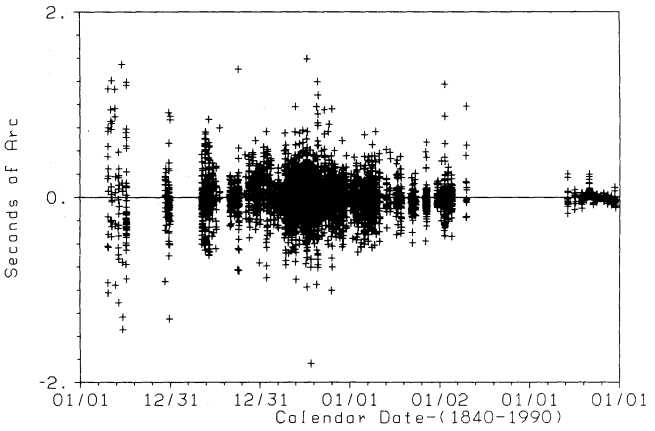

Fig. 2. Triton relative declination residuals

Table 2. Nereid observation residual statistics

Opp.	Observer	No.	Type	RMS	No.	Type	RMS
1949	van Biesbroeck	3	$\Delta\alpha \cos\delta$	1″.12	3	$\Delta\delta$	1″.29
1950	van Biesbroeck	7	$\Delta\alpha \cos\delta$	0″.512	8	$\Delta\delta$	0″.803
1951	van Biesbroeck	8	$\Delta\alpha \cos\delta$	0″.603	8	$\Delta\delta$	0″.885
1952	van Biesbroeck	3	$\Delta\alpha \cos\delta$	0″.805	3	$\Delta\delta$	0″.307
1953	van Biesbroeck	6	$\Delta\alpha \cos\delta$	0″.488	6	$\Delta\delta$	0″.439
1954	van Biesbroeck	4	$\Delta\alpha \cos\delta$	0″.420	4	$\Delta\delta$	0″.628
1955	van Biesbroeck	3	$\Delta\alpha \cos\delta$	0″.183	3	$\Delta\delta$	1″.11
1967	van Biesbroeck	5	$\Delta\alpha \cos\delta$	0″.895	5	$\Delta\delta$	0″.949
		1	α	1″.76	1	δ	0″.319
1968	van Biesbroeck	1	$\Delta\alpha \cos\delta$	0″.496	1	$\Delta\delta$	1″.36
		1	α	1″.49	1	δ	2″.25
1969	van Biesbroeck	3	$\Delta\alpha \cos\delta$	0″.891	3	$\Delta\delta$	2″.11
		1	α	1″.48	1	δ	0″.067
1977	Shelus	1	$\Delta\alpha \cos\delta$	0″.232	1	$\Delta\delta$	0″.299
1978	Mulholland	1	$\Delta\alpha \cos\delta$	0″.255	1	$\Delta\delta$	0″.369
1981	Veillet	4	$\Delta\alpha \cos\delta$	0″.108	4	$\Delta\delta$	0″.111
1982	Veillet	8	$\Delta\alpha \cos\delta$	0″.190	8	$\Delta\delta$	0″.120
1984	Veillet	3	$\Delta\alpha \cos\delta$	0″.117	3	$\Delta\delta$	0″.230
1987	Landgraf	5	$\Delta\alpha \cos\delta$	0″.497	5	$\Delta\delta$	0″.650
	Schaefer	4	α	0″.134	4	δ	0″.043
1988	Pascu	2	p	0°.114	2	s	0″.389
1989	Voyager	83	pixel	0″.203	83	line	0″.265

Table 3. Barycentric satellite state vectors at Julian ephemeris date 2447680.5 referred to the Earth mean equator and equinox of 1950.0

Satellite	R(km)	V(km s^{-1})
Triton	302505.012402645880	−1.44605178086895959
	75419.994387407661	−2.14769591843686046
	−169136.137125737224	−3.54389348775308512
Nereid	−2478165.52358444727	−0.275068314614426190
	4458349.93395644603	−0.948661370848684769
	2136966.64424202155	−0.506809954964708628

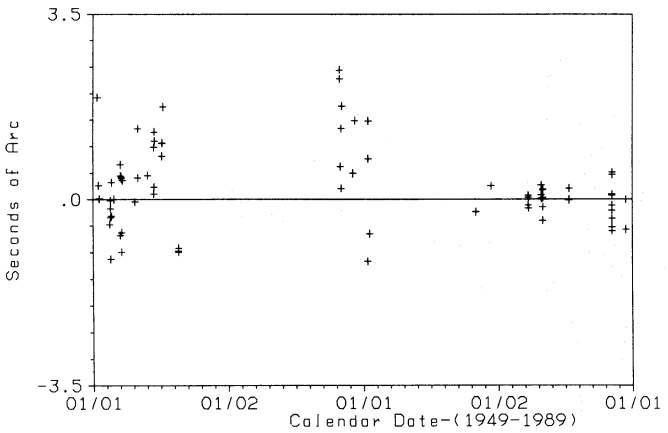

Fig. 3. Nereid relative right ascension residuals

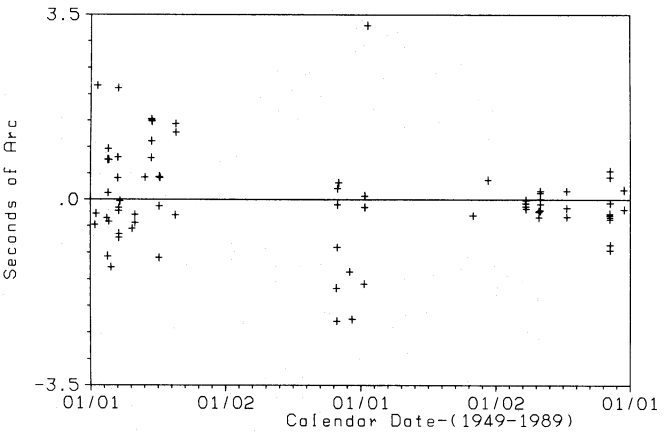

Fig. 4. Nereid relative declination residuals

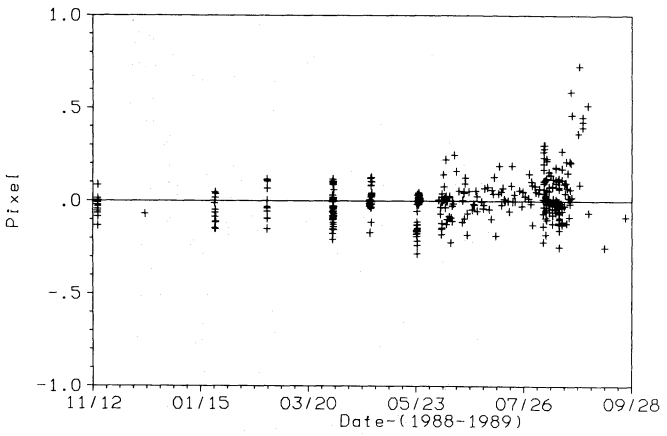

Fig. 5. Triton optical residuals

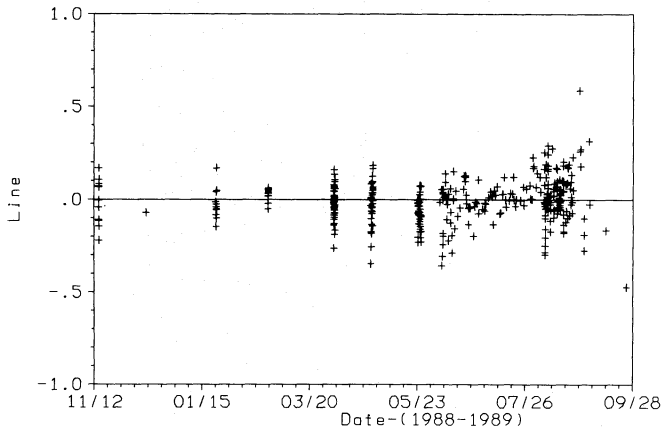

Fig. 6. Triton optical residuals

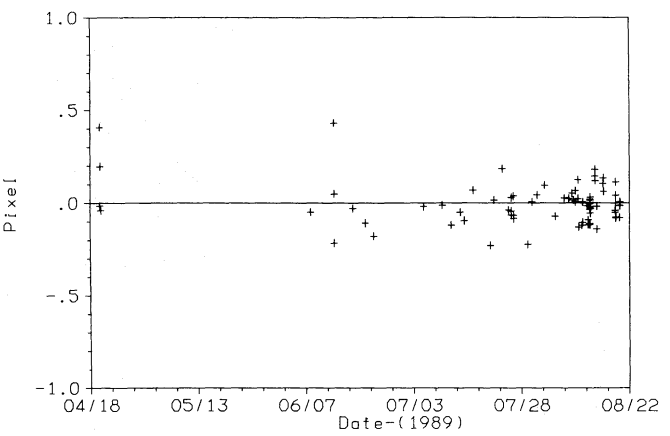

Fig. 7. Nereid optical residuals

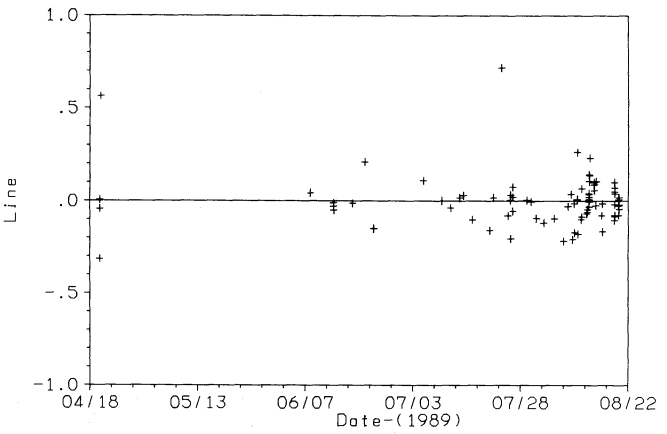

Fig. 8. Nereid optical residuals

through the system angular momentum. Since there is no direct source of information on the Neptune pole right ascension, it is determined from the angular momentum relationship. Consequently, it and the precession axis right ascension have the same uncertainty and are highly correlated. For the declination of Neptune's pole, direct information is available from the spacecraft radiometric tracking during the Neptune close approach. This information determines the Neptue pole but cannot be used to improve knowledge of the precession axis declination because of the uncertainties in Neptune spin rate and moment of inertia which enter into the angular momentum relationship.

5. Mean orbital elements

Because integrated orbits in terms of cartesian coordinates are difficult to interpret geometrically, an alternative qualitative representation of them in the form of mean orbital elements is often useful. The mean retrograde equinoctial elements for Triton appear in Table 5, and the mean direct equinoctial elements for Nereid appear in Table 6. In addition to the equinoctials, the tables give the classical elements derived from them. The Triton elements describe a planetocentric orbit whereas the Nereid elements describe a barycentric orbit. The reference plane for each satellite is its respective invariable plane, i.e., the plane on which its orbit precesses almost uniformly. All longitudes are measured from the node of the reference plane on the Earth mean equator of 1950.0. We obtained the elements by fitting precessing ellipse orbit models to the integrated orbits over the 151 year period from 9 September 1847 to 1 January 1989. Each fit included a determination of the pole of the satellite's invariable plane. For Triton this pole should be coincident with the Neptune pole precession axis (the system angular momentum vector). A comparison of the values of the orientation angles in Table 5 with those in Table 4 shows quite favorable agreement.

6. Relation to the Voyager navigation reconstruction

The orbits presented in this article are a refinement of those developed as part of the Voyager navigation reconstruction effort. The refinement was necessary because the orbits from the reconstruction, while quite accurate for the encounter period, did not provide an acceptable fit to the astrometric observations outside that period. In addition, the reconstruction did not determine the pole precession axis orientation or precession rate, i.e., the angular momentum constraint was not applied. In obtaining the current orbits, we used the reconstruction orbits as

Table 4. Neptunian system dynamical constants

Name	Value and actual uncertainty	Units
Neptune system GM	6836534.87889192492 ± 15	(km^3/s^2)
Triton GM	1427.86794914113370 ± 3.5	(km^3/s^2)
Nereid GM[a]	0.0	(km^3/s^2)
External body GM[b]	132883680730.629637	(km^3/s^2)
Neptune J_2	$(3410.47359149002860 \pm 9) \times 10^{-6}$	
Neptune J_4	$(-34.7030857830163906 \pm 10) \times 10^{-6}$	
Neptune radius[a]	25225	(km)
Triton radius[a]	1350 ± 7	(km)
Neptune pole right ascension[c]	298.857487705461094 ± 0.15	(deg)
Neptune pole declination[c]	42.8117932728048406 ± 0.05	(deg)
Precession axis right ascension	298.952582948808668 ± 0.15	(deg)
Precession axis declination	43.3134501284893594 ± 0.10	(deg)
Precession rate	52.3180099512911915 ± 0.25	(deg/cent)
Neptune period of rotation[a]	16.11 ± 0.02	(h)
Neptune moment of inertia ratio[a]	0.21 ± 0.01	

[a] Voyager adopted constants
[b] From DE130
[c] At Julian ephemeris date 2447763.5 (Voyager encounter date)

Table 5. Triton planetocentric mean elements at Julian ephemeris date 2447763.5 referred to the Triton invariable plane

Element	Value	Units
Semi-major axis	354759.146	(km)
$e \sin(\omega - \Omega)$	$+0.218348542 \times 10^{-5}$	
$e \cos(\omega - \Omega)$	$-0.154364851 \times 10^{-4}$	
$M + \omega - \Omega$	76.7243689	(deg)
$\cot(i/2) \sin \Omega$	+0.0281813825	
$\cot(i/2) \cos \Omega$	−0.2030103396	
$\dot{M} + \dot{\omega} - \dot{\Omega}$	61.2572637	(deg/day)
$\dot{\omega} - \dot{\Omega}$	0.382463540	(deg/yr)
$\dot{\Omega}$	0.523159764	(deg/yr)
Invariable plane pole right ascension	298.947294	(deg)
Invariable plane pole declination	43.3189060	(deg)
e	0.000015691	
$\omega - \Omega$	169.670538	(deg)
i	156.834472	(deg)
Ω	172.096852	(deg)

Table 6. Nereid barycentric mean elements at Julian ephemeris date 2433680.5 referred to the Nereid invariable plane

Element	Value	Units
Semi-major axis	5513413.256	(km)
$e \sin(\omega + \Omega)$	−0.724953400	
$e \cos(\omega + \Omega)$	−0.196840797	
$M + \omega + \Omega$	254.150289	(deg)
$\tan(i/2) \sin \Omega$	−0.0277252165	
$\tan(i/2) \cos \Omega$	+0.0567926008	
$\dot{M} + \dot{\omega} + \dot{\Omega}$	0.999624080	(deg/day)
$\dot{\omega} + \dot{\Omega}$	0.706322818	(deg/cent)
$\dot{\Omega}$	−3.91660963	(deg/cent)
Invariable plane pole right ascension	270.203984	(deg)
Invariable plane pole declination	69.1543762	(deg)
e	0.751201525	
$\omega + \Omega$	254.809177	(deg)
i	7.23242919	(deg)
Ω	333.979128	(deg)

our nominals and refit all of the data as previously discussed. Hence, the current orbits may be regarded as an iteration upon the reconstruction result.

The iteration improved the astrometric data fit, determined all the parameters in the precessing pole model, changed Triton's orbit during the encounter period by less than 3 km, and changed Nereid's orbit by less than 65 km. It also introduced statistically insignificant changes into the Neptunian system dynamical parameters. The parameter changes may be seen by comparing the values in Table 4 with the values given by Lewis (1990).

7. Comparison with the pre-encounter orbits

Figures 9 and 10 display the differences between the post-encounter orbits and the pre-encounter orbits (Paper II). The first figure shows the Triton in-orbit (V), radial distance (R), and out-of-plane differences (H) for the 24-day period centered on the Voyager Neptune encounter time. The largest difference is of the order of 500 km in the radial direction; the in-orbit difference is about 450 km, and the out-of-plane difference is about 200 km. The second figure shows the Nereid differences for the 120 day period beginning at the integration epoch and extending through the encounter. The largest difference is about 69,000 km in the in-orbit direction, the radial difference approaches 31,000 km, and the out-of-plane difference is nearly 11,000 km. All differences are well within the pre-encounter orbit uncertainties of 1100 km for Triton and 200,000 km for Nereid.

Comparing Triton's mean elements with those in Paper II shows that the semi-major axis has increased by 147 km, the eccentricity decreased by more than an order of magnitude, and the inclination to the invariable plane decreased by nearly 1 deg. The inclination change, however, is not due entirely to a reorientation of Triton's orbit in inertial space but rather is mostly the result of the nearly 1 deg increase in the declination of the invariable plane. The semi-major axis increase seems inconsistent with the mean radial distance increase of about 400 km. The apparent inconsistency is a consequence of comparing a planetocentric orbit semi-major axis with a barycentric orbit radial distance. The decrease in Triton's GM caused the planet to move about 250 km closer to the barycenter, and that move coupled with the semi-major axis increase lead to the 400 km radial distance increase. The amplitude of the periodic in-orbit and radial distance differences in Fig. 9 is a directly related to the eccentricity decrease, and amplitude of the periodic out-of-plane differences relates to the combination of small inclination and ascending node changes.

A comparison of Nereid's mean elements with those in Paper II shows an increase of about 2000 km in semi-major axis and a slight increase in eccentricity. These two changes combine to reduce the periapsis distance by about 1000 km. The mean anomaly at epoch increased about 0.3 deg which corresponds to a decrease in the time of periapsis passage of about 7.2 h. Directly related to this change in time of periapsis are the peak radial distance and in-orbit differences seen in Fig. 10. The former occurring at the ends of the latus rectum where the radial velocity is maximum, and the latter occurring at periapsis where the in-orbit velocity is maximum. Direct comparison of the orbit plane orientation angles is not possible because Paper II used the orbit plane of Saturn as its reference plane. However, the out-of-plane differences in Fig. 10 are consistent with a relative orbit inclination change of about 0.065 deg.

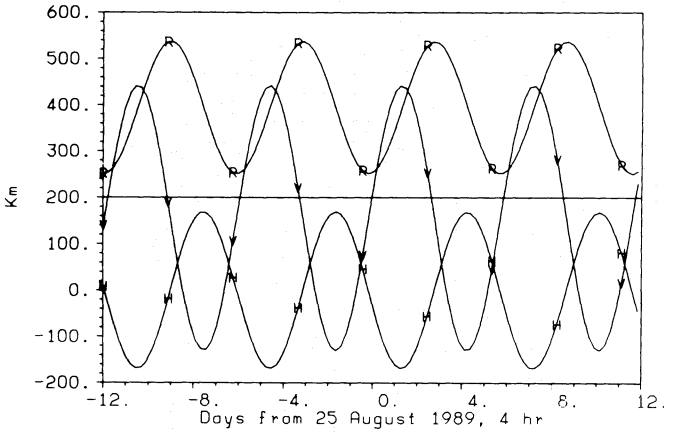

Fig. 9. Triton orbit differences

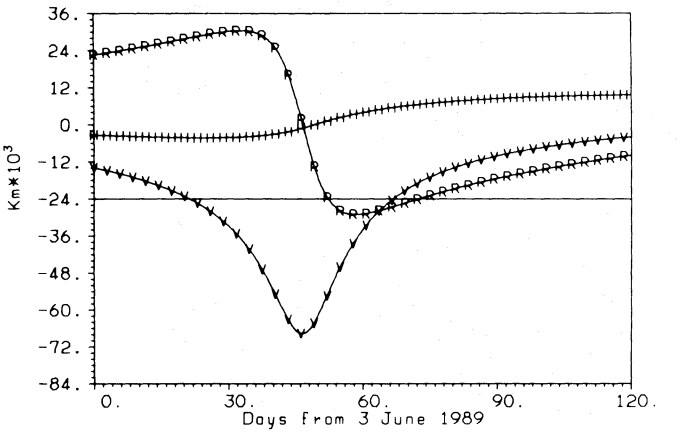

Fig. 10. Nereid orbit differences

8. Accuracy of the orbits

Figure 11 is a plot of the orbit uncertainty for Triton during the 24 day period surrounding the Voyager Neptune encounter, and Fig. 12 shows the orbit uncertainty for Nereid for the 2 year period beginning 3 June 1989. The figures display the orbit uncertainty in the in-orbit (V), radial distance (R), and out-of-plane (H) directions. The maximum uncertainties, in km, are about:

Sat.	V(km)	R(km)	H(km)
Triton	40	13	45
Nereid	1900	800	500

The maximum Nereid uncertainty occurs at a sharply defined peak in the vicinity of periapsis in 1990. No similar peak occurs in 1989 (approximately one orbital period earlier) because the orbit was well determined at that time from the high quality Voyager optical data. Propagation of the 1989 orbit to 1990 and beyond is degraded by the relatively poor knowledge of Nereid's period. In fact, the in-orbit error for both satellites will grow with time due to the errors in their orbital periods. The table below gives the estimated period errors and associated increase in in-orbit uncertainty:

Sat.	Period error	Error growth
Triton	0.4 s	100 km/yr
Nereid	10 min	1850 km/yr

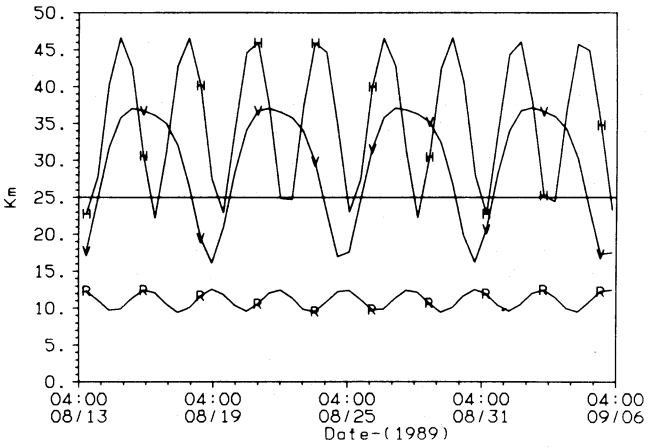

Fig. 11. Triton orbit sigmas

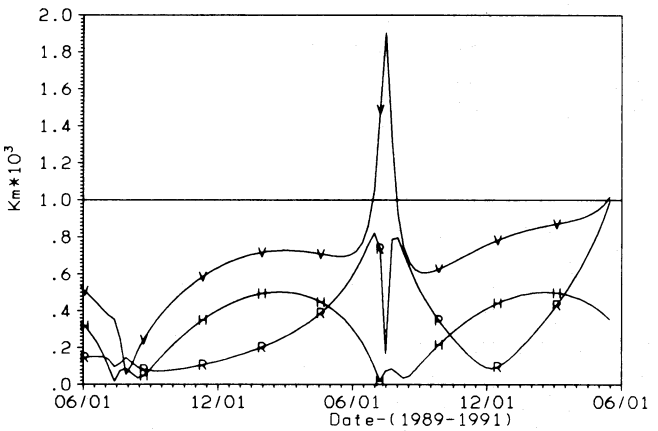

Fig. 12. Nereid orbit sigmas

9. Concluding remarks

This paper has reported on the determination of the orbits of the Neptunian satellites, Triton and Nereid, using a numerical integration fit to Earthbased astrometric satellite observations and to data obtained from the Voyager spacecraft. As a byproduct, the fit yielded new values for the Neptunian system GM, Triton's GM, the second and fourth zonal harmonics of the Neptune gravitational field, and the orientation of the Neptune pole. The orbits represent an improvement of those previously reported, and a comparison with the earlier orbits was included. Ephemerides based on the new orbits are available for support of future scientific investigations of the Neptunian system.

Acknowledgements. The research described in this paper was carried out at the Jet Propulsion Laboratory, California Institute of Technology, Pasadena CA under contract to the National Aeronautics and Space Administration. The authors wish to thank D. Pascu for providing unpublished Nereid astrometric observations.

Appendix A

The angular momentum of an axially symmetric planet can be written as:

$$\boldsymbol{H}_p = [(C\dot{W}) - A(\hat{h}\cdot\boldsymbol{\omega}_p)]\hat{h} + A\boldsymbol{\omega}_p$$

where
A = planet moment of inertia about the equatorial plane
C = planet moment of inertia about the pole
$\dot{W}$ = planet spin rate about the pole
$\hat{h}$ = unit vector along the planet pole
$\boldsymbol{\omega}_p$ = angular velocity of the planet pole.
The polar moment of inertia can be expressed in the form:

$$C = \gamma m_0 R^2$$

where
m_0 = mass of the planet
R = equatorial radius of the planet
γ = the ratio of the axial moment of inertia to the moment of inertia of a homogeneous sphere having the planet's mass and a radius equal to the planet's equatorial radius.
The two moments of inertia are related by the expression:

$$A = (\gamma - J_2)m_0 R^2$$

where J_2 is the second zonal harmonic of the planet gravitational potential.

The angular momentum of a system composed a planet and n satellites (ignoring the rotational momentum of the satellites) is:

$$\boldsymbol{H} = \boldsymbol{H}_p + \sum_{i=1}^{n} m_i(\boldsymbol{r}_i - \boldsymbol{r}_0) \times \boldsymbol{v}_i$$

where
m_i = mass of satellite i
$\boldsymbol{r}_0$ = barycentric position of the planet
$\boldsymbol{r}_i$ = barycentric position of satellite i
$\boldsymbol{v}_i$ = barycentric velocity of satellite i,
Due to the torque exerted by the satellites, the angular momentum vector of the planet precesses about the system angular momentum vector. If constant precession is assumed, the angular velocity of the pole becomes:

$$\boldsymbol{\omega}_p = \dot{\psi}\hat{k}$$

where
$\dot{\psi}$ = the precession rate
$\hat{k}$ = the unit vector aligned with $\boldsymbol{H}$.

References

Bierman G.J., Nead M.W., 1978, "A Parameter Estimation Subroutine Package", Jet Propulsion Laboratory Publication 77-26, Rev. 2, Jet Propulsion Laboratory, Pasadena, California

Gerschultz J.W., 1989, "PHYSCON-8 Inputs Meeting", IOM VGR-JWG-89-036, Jet Propulsion Laboratory, Pasadena, California (Internal Document)

Holberg J.B., 1990 (private communication of unpublished Voyager UVS occultation times)

Jacobson R.A., Lewis G.D., Riedel J.E., Roth D.C., Synnott S.P., Taylor A.H., 1986, Am. Inst. Aeronaut. Astronaut. Paper 86-2059-CP, Am. Inst. Aeronaut. Astronaut./Am. Astronaut. Soc. Astrodynamics Conference, Williamsburg, Virginia

Jacobson R.A., 1987, Am. Astronaut. Soc. Paper 87-464, Am. Astronaut. Soc./Am. Inst. Aeronaut. Astronaut. Astrodynamics Conference, Kalispell, Montana

Jacobson R.A., 1990, A&A 231, 241

Lewis G.D., Taylor A.H., Jacobson R.A., Roth D.C., Riedel J.E., Synnott S.P., Ryne M.S., 1990, Am. Inst. Aeronaut. Astronaut. Paper 90-2879, Am. Inst. Aeronaut. Astronaut./Am. Astronaut. Soc. Astrodynamics Conference, Portland, Oregon

Lawson C.L., Hanson R.J., 1974, Solving Least Squares Problems, Prentice-Hall, Englewood Cliffs, New Jersey

Marouf E.A., 1990 (private communication of unpublished Voyager RSS occultation times)

Pascu D., 1989 (private communication of unpublished USNO observations)

Peters C.F., 1981, A&A 104, 37

Riedel J.E., Owen W.M., Stuve J.A., Synnott S.P., Vaughan R.M., 1990, Am. Inst. Aeronaut. Astronaut. Paper 90-2877, Am. Inst. Aeronaut. Astronaut./Am. Astronaut. Soc. Astrodynamics Conference, Portland, Oregon

Standish E.M., 1987, Ephemerides, DE130/LE130 and DE202/LE202. IOM 314.6-891, Jet Propulsion Laboratory, Pasadena, California (Internal Document)

Synnott S.P., Donegan A.J., Riedel J.E., Stuve J.A., 1986, Am. Inst. Aeronaut. Astronaut. Paper 86-2113-CP, Am. Inst. Aeronaut. Astronaut./Am. Astronaut. Soc. Astrodynamics Conference, Williamsburg, Virginia

Taylor A.H., Jacobson R.A., Synnott S.P., Lewis G.D., Riedel J.E., Roth D.C., 1986, Am. Inst. Aeronaut. Astronaut. Paper 86-2112-CP, Am. Inst. Aeronaut. Astronaut./Am. Astronaut. Soc. Astrodynamics Conference, Williamsburg, Virginia